

## MIT Open Access Articles

*A CRISPR-based assay for the detection of opportunistic infections post-transplantation and for the monitoring of transplant rejection*

The MIT Faculty has made this article openly available. **Please share** how this access benefits you. Your story matters.

**Citation:** Kaminski, Michael M. et al. "A CRISPR-based assay for the detection of opportunistic infections post-transplantation and for the monitoring of transplant rejection." *Nature Biomedical Engineering* 4, 6 (April 2020): 601–609 © 2020 The Author(s)

**As Published:** <http://dx.doi.org/10.1038/s41551-020-0546-5>

**Publisher:** Springer Science and Business Media LLC

**Persistent URL:** <https://hdl.handle.net/1721.1/125918>

**Version:** Author's final manuscript: final author's manuscript post peer review, without publisher's formatting or copy editing

**Terms of use:** Creative Commons Attribution-Noncommercial-Share Alike



1 **A CRISPR-based assay for the detection of opportunistic infections post-transplantation and for**  
2 **the monitoring of transplant rejection**  
3

4 Michael M. Kaminski<sup>1,2,3</sup>, Miguel A. Alcantar<sup>1</sup>, Isadora Lape<sup>4</sup>, Robert Greensmith<sup>2,3</sup>, Allison C.  
5 Huske<sup>1</sup>, Jacqueline A. Valeri<sup>1,9</sup>, Francisco M. Marty<sup>5</sup>, Verena Klämbt<sup>6</sup>, Jamil Azzi<sup>4</sup>, Enver  
6 Akalin<sup>7</sup>, Leonardo V. Riella<sup>4\*</sup>, and James J. Collins<sup>1,8,9\*</sup>  
7  
8

9 **Abstract**

10 **In organ transplantation, infection and rejection are major causes of graft loss linked by**  
11 **the net state of immunosuppression. To diagnose and treat these conditions earlier, and**  
12 **to improve long-term patient outcomes, refined strategies for the monitoring of patients**  
13 **after graft transplantation are needed. Here, we show that a fast and inexpensive assay**  
14 **based on CRISPR-Cas13 accurately detects BK polyomavirus DNA and cytomegalovirus**  
15 **DNA from patient-derived blood and urine samples, as well as CXCL9 mRNA (a marker of**  
16 **graft rejection) at elevated levels in urine samples from patients experiencing acute**  
17 **renal-transplant rejection. The assay, which we adapted for lateral-flow readout, enables**  
18 **via simple visualization the post-transplantation monitoring of common opportunistic**  
19 **viral infections and of graft rejection, and should facilitate point-of-care post-**  
20 **transplantation monitoring.**  
21  
22

23 <sup>1</sup>Institute for Medical Engineering and Science and Department of Biological Engineering, Massachusetts Institute of Technology,  
24 Cambridge, MA 02139, USA. <sup>2</sup>Berlin Institute for Medical Systems Biology, Max Delbrück Center for Molecular Medicine in the  
25 Helmholtz Association, 10115 Berlin, Germany. <sup>3</sup>Department of Nephrology and Medical Intensive Care, Charité -  
26 Universitätsmedizin Berlin, 10117 Berlin, Germany. <sup>4</sup>Schuster Transplantation Research Center, Brigham & Women's Hospital,  
27 Harvard Medical School, Boston, MA 02115, USA. <sup>5</sup>Division of Infectious Diseases, Brigham and Women's Hospital, Boston, MA  
28 02115, USA. <sup>6</sup>Department of Medicine, Boston Children's Hospital, Harvard Medical School, Boston, MA 02115, USA. <sup>7</sup>Montefiore  
29 Einstein Center for Transplantation, Montefiore Medical Center, Albert Einstein College of Medicine, Bronx, New York 10467, USA.  
30 <sup>8</sup>Infectious Disease and Microbiome Program, Broad Institute of MIT and Harvard, Cambridge, MA 02142, USA. <sup>9</sup>Wyss Institute for  
31 Biologically Inspired Engineering, Harvard University, Boston, MA 02115, USA. \*corresponding authors, e-mail: [jimjc@mit.edu](mailto:jimjc@mit.edu),  
32 [lrliella@bwh.harvard.edu](mailto:lrliella@bwh.harvard.edu)  
33

34 **Main**

35 The clustered regularly interspaced short palindromic repeats (CRISPR) and CRISPR-  
36 associated (Cas) immune system has recently been adapted for the detection of nucleic acids<sup>1-</sup>  
37 <sup>8</sup>. These protocols enable rapid, cost-effective DNA and RNA detection in a variety of sample

38 types with excellent sensitivity and specificity, making them ideal tools for point-of-care (POC)  
39 testing. However, most studies to date have used synthetic standards, include few clinical  
40 specimens, and lack direct comparison to clinical gold standard diagnostics.

41 Here, we applied and optimized the CRISPR-Cas13 SHERLOCK (specific high-sensitivity  
42 enzymatic reporter unlocking) technology for diagnosis of biomarkers highly relevant for renal  
43 transplant patients.

44

45 Since the first successful kidney transplantation in 1954, significant improvements in short-term  
46 outcomes have been achieved in organ transplantation. However, there has been less progress  
47 in long-term outcomes with more than half of the transplanted organs being lost after 10  
48 years<sup>9,10</sup>. Opportunistic infections and transplant organ rejection are leading causes of graft loss,  
49 requiring careful adjustment of immunosuppression and life-long monitoring of post-transplant  
50 patients<sup>11</sup>.

51

52 Current diagnostics, however, involve the use of expensive laboratory equipment and intricate  
53 multi-step protocols leading to limited availability, high costs and slow turn-around time<sup>12,13</sup>.

54 Diagnosis of infections by PCR can take several days in clinical settings, and rejection  
55 diagnostics require invasive biopsies and histopathological analysis. These factors result in  
56 delays in pertinent diagnoses and increase the risk of irreversible allograft injury, especially in  
57 resource-limited settings. POC or at-home testing could significantly reduce associated costs  
58 and allow for more frequent monitoring, which would lead to earlier diagnosis and treatment of  
59 graft dysfunction and common infections.

60

61 In this study, we developed CRISPR-based diagnostic tools for cytomegalovirus (CMV) and BK  
62 polyomavirus (BKV) infection, two common opportunistic viruses highly relevant for renal  
63 transplant patients<sup>14</sup> and other immunocompromised patients<sup>15,16</sup>. Testing of more than 100  
64 clinical specimens from BKV and CMV infected patients over a wide range of virus loads  
65 revealed high diagnostic accuracy. We further extended the capability of SHERLOCK to the  
66 detection of human *CXCL9* mRNA, a biomarker indicative of rejection in renal transplant  
67 patients<sup>17-19</sup>. We anticipate that CRISPR-Cas13-based technologies will be broadly applicable  
68 for personalized medicine diagnostics, where repeated testing of biomarkers indicative of  
69 disease activity is key to early and effective secondary prevention.

70

71

72 **Results**

73 **Optimization of the CRISPR-Cas13 SHERLOCK technology for the detection of BKV and**  
74 **CMV virus from patient samples**

75 To test for active BKV and CMV infection, we isolated DNA from blood and urine of both  
76 infected patients and uninfected control patients (Fig. 1a). Subsequently, we applied a modified  
77 version of the SHERLOCK protocol for BKV and CMV detection. In brief, conserved regions of  
78 BKV and CMV were amplified using isothermal recombinase polymerase amplification (RPA).  
79 Incorporation of the T7 promoter sequence into forward primers allowed for subsequent in-vitro  
80 RNA transcription using T7 polymerase. A CRISPR guide RNA (crRNA) complimentary to 28  
81 nucleotides of the RPA product was used to direct Cas13 from *Leptotrichia wadei* (LwaCas13a)  
82 to the target sequence. Detection of the target resulted in Cas13 activation and subsequent  
83 collateral cleavage of an oligonucleotide carrying a quenched fluorophore, whose fluorescence  
84 can be measured upon cleavage and correlates with the initial target concentration present in  
85 the patient sample<sup>1</sup>.

86  
87 To identify conserved regions in the BKV genome, we aligned all strains accessible from the  
88 National Center for Biotechnology Information (NCBI) and focused on target regions with  
89 sequence homology of more than 95% among all strains (Fig. 1b). Next, we tested 12 different  
90 primer pairs and 3 crRNAs for detection of the BKV genes STA, VP2 and VP3 (Supplementary  
91 Fig.1a). We identified a crRNA-primer pair specific for the small T antigen (STA), which allowed  
92 detection of the *American Type Culture Collection* (ATCC) quantitative synthetic BKV standard  
93 (Dunlop strain) down to the low atto-molar range (0.3 aM), representing single-molecule  
94 detection in the assay volumes used (Figs. 1c,d). Importantly, systematic assessment of various  
95 forward and reverse primer concentrations (Supplementary Fig.1b) revealed a 120/480nM  
96 forward/reverse RPA primer concentration to be most sensitive. Using a similar strategy, we  
97 identified a conserved region in the CMV UL54 gene (Fig. 1e) as a potential SHERLOCK target  
98 which enabled detection of the ATCC diagnostic CMV standard (strain AD-169) down to the low  
99 atto-molar range (0.6 aM) (Figs. 1f,g).

100

101 Next, we tested if the diagnostic performance of the SHERLOCK assay would be sufficient to  
102 detect BKV and CMV virus in urine and plasma samples from patients. Testing of 31 urine and  
103 36 plasma samples showed that the optimized SHERLOCK protocol correctly identified all BKV  
104 specimens with 100% sensitivity and specificity (Figs 2a,b, Supplementary Fig.2a). Importantly,  
105 this performance could be achieved using the rapid and simple HUDSON (heating unextracted

106 diagnostic samples to obliterate nucleases) protocol<sup>2</sup>, which involves heating of the sample for  
107 10 min at 95°C in the presence of TCEP and EDTA, circumventing the need for time-  
108 consuming, column-based sample preparations (Supplementary Figs. 2b,c).

109  
110 Similarly, the CRISPR assay allowed for detection of CMV positive plasma samples with high  
111 sensitivity and specificity (Figs. 2c,d, Supplementary Figs.2b,c). In contrast to our BKV results,  
112 this performance could only be achieved using a commercial column-based viral DNA isolation  
113 kit, whereas the HUDSON protocol resulted in lower sensitivity for low copy number samples (<  
114 1500 IU/mL). Likely, this difference in sensitivity is due to a sample concentration step included  
115 in the column-based kit.

### 116 117 **CRISPR-based detection of *CXCL9* mRNA as a biomarker of kidney graft rejection**

118 Next, we tested whether SHERLOCK could be applied to detect mRNA biomarkers indicative of  
119 kidney graft rejection. We selected *CXCL9* mRNA as a marker of rejection based on its  
120 validation in multicenter studies<sup>17,18,20</sup>.

121  
122 For detection of *CXCL9* mRNA, we isolated RNA from pelleted urine cells (Fig. 3a). For  
123 amplification, we included a reverse transcriptase into the RPA reaction (rtRPA). Using a  
124 synthetic RNA standard, Cas13 alone was sufficient to detect *CXCL9* in the low pico-molar  
125 range similar to the previously reported sensitivity (Fig. 3b). Addition of a rtRPA reaction  
126 followed by T7 transcription and Cas13 activation enabled *CXCL9* detection in the atto-molar  
127 range (Fig. 3b).

128  
129 We next assessed whether this sensitivity was sufficient to discriminate patients undergoing  
130 kidney rejection (n=14) from a control group (n=17) (Supplementary Table 1). Importantly,  
131 rejection status was determined by gold standard kidney biopsy (Supplementary Table 2).  
132 We observed higher *CXCL9* mRNA levels in samples from patients with biopsy-proven rejection  
133 compared to transplant patients with no rejection or stable graft function, which allowed for the  
134 detection of kidney rejection with a sensitivity of 93% (Figs. 3c,d). The area under the receiver-  
135 operating-characteristic (ROC) curve (AUC) was 0.91 (Fig. 3e).

136  
137 We confirmed *CXCL9* mRNA upregulation in rejection samples with the qPCR gold-standard  
138 assay<sup>18</sup> observing higher diagnostic accuracy relative to the CRISPR-based assay  
139 (Supplementary Figs. 3a,b,c). Detection of *CXCL9* protein with an enzyme-linked

140 immunosorbent assay (ELISA) showed lower sensitivity but higher specificity (Supplementary  
141 Figs. 3d,e,f) as compared to CRISPR-based mRNA detection.

142  
143 **Rapid DNA isolation, CRISPR diagnostics and smartphone-based lateral-flow evaluation**  
144 **allow POC-ready detection of BKV and CMV infection**

145 Point-of-care testing (POCT) holds great promise for transplantation medicine since fast and  
146 low-cost diagnostics could enable earlier treatment decisions and broader accessibility, thereby  
147 lowering the risk of irreversible transplant injury. To optimize BKV and CMV detection for POCT,  
148 we combined the rapid HUDSON DNA isolation protocol with SHERLOCK-based target  
149 detection and commercially available lateral-flow dipsticks (Fig. 4a). This method enabled an  
150 easy-to-read visual output that indicated a positive or negative test result. Since we observed  
151 that background noise can result in a faint test band on the lateral flow strip, we developed a  
152 smartphone-based software application that allowed quantification of band intensities  
153 (Supplementary video 1). Here, the software calculates the ratio of test to control band  
154 intensities using images taken with a smartphone camera, enabling simple and rapid  
155 discrimination between negative and positive test results. The total turn-around time from  
156 isolation to sample detection was below 2 hours.

157  
158 We next tested the lateral-flow read-out for the detection of the CMV and BKV synthetic  
159 standard (Figs. 4b,c). Similar to our fluorescence-based read-out, we could detect both targets  
160 down to the atto-molar range. We set the relative band intensity cut-off discriminating a positive  
161 from a negative test result to 0.5, which corresponded to an interpolated concentration of 2.3 aM  
162 for the CMV standard and 0.5 aM for the BKV standard.

163  
164 Using this protocol, we were able to detect CMV (Fig. 4d) and BKV (Fig. 4e) at different  
165 concentrations in patient samples. Although faint test bands were observable at very low  
166 concentrations, they were below the band intensity cut-off and thus classified as negative.  
167 Further, lateral flow-based CRISPR diagnostics successfully identified BKV infection in a 58-  
168 year-old male kidney transplant patient who was admitted for graft dysfunction. A kidney biopsy  
169 demonstrated BKV nephropathy and qPCR confirmed high viral BKV titers in the blood.  
170 After treatment, we could not detect BKV using CRISPR-Cas13 which was confirmed by the  
171 absence of viral DNA in qPCR (Fig. 4f).

172

173 To assess lateral-flow signal variability over time, we tested the same ten BKV positive or  
174 negative patient samples on three different days (Figs. 4g,h). We observed that all BKV  
175 negative samples were consistently below the band intensity cut-off on the three different days,  
176 whereas all BKV positive samples were above. This suggested a low variability of background  
177 noise and band intensities.

178  
179 We also assessed the influence of incubation time and temperature on lateral-flow band  
180 intensity for two different concentrations of the CMV synthetic standard. For the negative  
181 control, the relative band intensity stayed below the 0.5 cut-off regardless of the incubation time,  
182 similar to our previous results (Supplementary Figs. 4a,b). When detecting 5 or 500 aM of CMV  
183 synthetic DNA, we observed a time-dependent increase of band intensities. Importantly, we  
184 could observe band intensity values above the cut-off only after 60 min, indicating that our  
185 assay incubation time could be further shortened. For different reaction temperatures ranging  
186 from 21°C to 39°C, we again observed band intensity ratios below 0.5 for the negative control  
187 (Supplementary Figs. 4c,d). While room temperature (21°C) was sufficient to detect 5 and 500  
188 aM of CMV synthetic standard, higher temperatures correlated with higher band intensities.  
189 These results indicate that reaction time and temperature are important variables if a  
190 quantitative lateral flow read-out is the goal. In contrast, highly consistent background noise  
191 irrespective of daily variation, incubation time and temperature enables a robust qualitative  
192 assay.

193  
194 We further optimized the combination of RPA, T7 transcription and Cas13 in one reaction (“one-  
195 pot reaction”, Supplementary Fig. 5a) by testing different reaction buffers and nucleotide ratios  
196 (Supplementary Figs. 5b-d). Using this optimized one-pot reaction, we achieved BKV detection  
197 in the atto-molar range (Supplementary Fig. 5e).

198  
199 **Detection of *CXCL9* mRNA levels with lateral-flow enables monitoring of kidney rejection**  
200 **and treatment response**

201 Next, we sought to apply the lateral-flow-based assay for the detection of *CXCL9* mRNA  
202 indicative of acute cellular kidney rejection. Similar to the detection of viral DNA, lateral flow  
203 enabled robust detection of *CXCL9* synthetic RNA (Fig. 5a) down to the atto-molar range.  
204 Using nonlinear regression analysis, we determined that a concentration of 12 aM corresponded  
205 to the 0.5 band intensity cut-off.

206

207 In order to explore the power of our CRISPR-based read-out for rejection monitoring, we  
208 selected two patients experiencing allograft cellular rejection as confirmed by biopsy who had at  
209 least three prospective samples after the rejection event (Figs. 5b,c). Patient 1 (Fig. 5b)  
210 developed an acute cellular rejection (Banff IIA) and showed a good response to treatment with  
211 thymoglobulin and pulse methylprednisolone, achieving full clinical recovery. This was reflected  
212 by a strong downregulation of *CXCL9* mRNA levels as observed in qPCR and return to his  
213 baseline serum creatinine (0.9 mg/dL). CRISPR-based testing detected *CXCL9* mRNA only  
214 during rejection, while the patient was *CXCL9* negative after treatment completion.

215

216 In contrast, Patient 2 (Fig. 5c) had an episode of acute cellular rejection Banff IIA with partial  
217 improvement of creatinine after treatment (Serum creatinine 3.5 mg/dL down from 7.9). While  
218 urine *CXCL9* mRNA was reduced initially, it went back up 7 months afterwards, and repeat  
219 biopsy revealed chronic active cellular rejection. Overall, monitoring of urine *CXCL9* mRNA  
220 levels may be a useful tool to assess response to rejection treatment, though further validation  
221 in a larger trial is needed.

222

## 223 **Discussion**

224 Fast and cost-effective POCT should enable early diagnosis and greater accessibility for  
225 patients in low-resource settings, including the opportunity for self-monitoring. Here, we applied  
226 CRISPR-Cas13 diagnostics to detect CMV and BKV infection in samples of kidney transplant  
227 patients. We extended the use of SHERLOCK for the detection of *CXCL9* mRNA, a biomarker  
228 of acute cellular rejection of kidney transplants. Together, these developments may enable the  
229 cost-effective (Supplementary Table S3) monitoring of patients at risk for opportunistic infection  
230 and serve as a tool for earlier detection of rejection and monitoring post-treatment in  
231 transplantation.

232

233 BKV and CMV are among the most common opportunistic infections after solid-organ  
234 transplantation, being associated with significant morbidity<sup>21</sup>. However, clinical presentation is  
235 variable in transplanted patients and BKV infection frequently presents without clinical  
236 symptoms except a creatinine rise, which indicates already established BK nephropathy. Blood  
237 testing for BKV and CMV viral load is recommended but not uniformly performed in all centers  
238 due to cost limitations, in particular in developing countries. Here, our high-sensitivity, low-cost  
239 POC assay could allow for more frequent testing.

240



241 Rejection is the leading cause of chronic allograft loss. However, rejection is usually detected  
242 late since serum creatinine is a delayed marker of allograft injury. Furthermore, the diagnosis of  
243 acute rejection currently requires a renal biopsy - an invasive process that is limited by sampling  
244 error and assessment variability<sup>22</sup>. In order to detect graft injury earlier, some centers perform  
245 surveillance kidney biopsies at pre-specified time-points post-transplant<sup>23</sup>. However, these  
246 procedures are associated with major risks for patients, such as bleeding, and significant costs  
247 (~\$3,500/biopsy, which includes the procedure and the pathological analyses of the kidney  
248 specimen). Therefore, a sensitive and non-invasive assay such as CRISPR-Cas13-based  
249 *CXCL9* mRNA testing could allow for more frequent testing and thereby achieve earlier  
250 detection of graft rejection, allowing timely diagnosis and treatment.

251  
252 *Here, we focused on cellular-mediated rejection, the most frequent rejection affecting*  
253 *kidney transplant patients. Screening for donor-specific anti-HLA antibodies (DSA) is*  
254 *currently performed in patients with concern for antibody-mediated rejection. All patients*  
255 *included in our study had a negative test for DSA. Screening prospectively for DSA in*  
256 *all patients is not uniformly performed in part due to lack of specificity of DSA to*  
257 *antibody-mediated rejection<sup>24,25</sup>.*

258  
259 Two novel blood tests that detect the fraction of donor-derived cell-free DNA have become  
260 clinically available in kidney transplantation to monitor for rejection<sup>26,27</sup>. While these assays have  
261 shown promising results, they still require a visit to the clinic to draw blood, shipping of the  
262 material to outside labs for processing and analysis, and they have a high price tag of US  
263 \$2,821 per test<sup>28</sup>. This high price limits the frequency of testing and also prevents the use of this  
264 test in resource-limited settings. The advantages of our rejection assay are its low cost, its high  
265 sensitivity and its use of urine compared to blood. Since *CXCL9* mRNA elevation in the urine  
266 can be detected weeks before elevation of creatinine due to rejection<sup>29</sup>, urine *CXCL9* mRNA  
267 monitoring may represent a promising technique for earlier rejection detection as well as post-  
268 treatment monitoring. Lastly, the development of a smartphone application to enable simple and  
269 fast interpretation of the lateral-flow assay allows for sharing of results directly with the provider,  
270 leading to a convenient way of monitoring patients between clinical appointments.

271  
272 Our test was mainly aimed for the qualitative detection of CMV, BKV and *CXCL9* at clinically  
273 relevant concentrations. However, in many clinical situations, precise quantification of the viral

274 load and changes in biomarker levels are useful. Future iterations of this protocol should,  
275 therefore, include quantitation strategies and may build on recent protocols demonstrating semi-  
276 quantitative read-outs of CRISPR diagnostics<sup>3</sup>. This would also strengthen the power of  
277 CRISPR-based diagnostics, since it could allow for the detection of subtle changes as a  
278 deviation from an individualized baseline. Moreover, although most steps could be optimized for  
279 a POCT setting, sample isolation for the detection of mRNA still required a column-based  
280 approach. Thus, further work will consist in optimizing the protocol for simplified mRNA isolation  
281 procedures. In addition, heating represents an essential step in our current sample processing  
282 protocol using HUDSON. Thus, the integration of POC heating devices using chemical<sup>30</sup> or  
283 electromagnetic<sup>31</sup> heating might facilitate handling for the primary care provider or patient.  
284 Finally, inclusion of more patient samples and prospective analysis will allow for systematic  
285 comparison with current clinical practice.

286

287 In summary, this work demonstrates the application of CRISPR-Cas13 for the detection of  
288 rejection and opportunistic infection in kidney transplantation. This technology could be easily  
289 applied to other solid-organ transplants as well as immune-mediated kidney diseases such as  
290 lupus nephritis. Based on its low-cost, ease of use and speed, this assay could allow frequent  
291 testing and earlier diagnosis. The next steps in order to advance clinical implementation include  
292 studies to validate these findings and to demonstrate the clinical utility of this assay in regard to  
293 long-term outcomes of kidney transplant recipients.

294

## 295 **Methods**

296 **Lateral flow reactions.** 20µl of the Sherlock reaction containing the lateral flow reporter-oligo at  
297 1µM (sequence in supplementary table 4) were mixed with 80µl of Hybridetect Assay buffer,  
298 followed by insertion of lateral flow-sticks (Milenia Hybridetect1, TwistDx Limited, Maidenhead,  
299 UK) and incubation for 3min at room temperature, according to the manufacturer's instructions,  
300 before images were taken.

301 **Image analysis of lateral flow reactions.** The relative band intensities of each of the lateral-  
302 flow sticks were measured using ImageJ software (US National Institute of Health). The relative  
303 band intensity was calculated as the test band's mean grey value/control band's mean grey  
304 value. Images were first converted to 8-bit and inverted, before highlighting the band region and  
305 measuring its mean grey value.

306 **Lateral flow quantification app.** The lateral flow quantification algorithm was implemented  
307 using Python's opencv package (v4.1.1). Briefly, images uploaded to the app are automatically

308 converted to grayscale and the colors are inverted. The resultant image is then subjected to a  
309 Gaussian blur in order to remove outlier pixels that may result in artifactual bright-spots.  
310 Afterward, a threshold is applied to accentuate bright spots. Connected component analysis is  
311 then used to isolate regions corresponding to the control and sample bands. These bands are  
312 then identified and quantified by calculating the mean intensity of each band. If the sample band  
313 cannot be identified due to weak intensity, the sample band's location is estimated by scanning  
314 for bright areas in the upper portion of the lateral flow stick using the control band as a  
315 perspective scale. The ratio of the sample to control band is then calculated and displayed to  
316 the user. The Android app was developed with Android Studio v3.5.1 (Google, Mountain View,  
317 CA) with Java 8 and Gradle v5.4.1 (Supplementary Video 1). To provide a clean user interface,  
318 the main screen was limited to three buttons: (1) upload new pictures, (2) specify the target of  
319 the assay (i.e., CMV, BKV, or CXCL9), and (3) initiate image analysis. The picture upload  
320 process requests read permissions of the phone's photo gallery. Image analysis allows for two  
321 options, with the faster analysis scaling down the image to 50% lower resolution for more rapid  
322 results. The pixel array is passed to a Python backend through Chaquopy v6.3.0, a Python SDK  
323 for Android.

324 **Sample preparation.** Patient samples containing CMV or BKV were prepared as indicated,  
325 either with the previously described HUDSON protocol<sup>2</sup> or the QIAamp MinElute Virus Spin Kit  
326 (Qiagen, Hilden, Germany), according to the manufacturer's instructions. For HUDSON  
327 processing, the samples were heated for 10min at 95°C in the presence of 100mM TCEP  
328 (Fisher Scientific, USA) and 1mM EDTA (Fisher Scientific, USA). For CXCL9 mRNA detection,  
329 45 ml urine was centrifuged for 30min at 2000g at 4°C, followed by washing of the pellet with  
330 PBS and resuspension in 200µl RNeasy Lysis Buffer (Qiagen, Hilden, Germany). All samples were  
331 aliquoted and stored at -80°C. RNA was isolated using the RNeasy Micro Kit (Qiagen, Hilden,  
332 Germany) and the PureLink RNA Mini Kit (Invitrogen, USA), following the manufacturer's  
333 instructions.

334 **Production of crRNAs and LwaCas13a.** LwaCas13a was produced by Genscript (Piscataway,  
335 USA). crRNAs were synthesized using the HiScribe™ T7 Quick High Yield RNA Synthesis Kit  
336 (NEB, Ipswich, USA), according to the manufacturer's instructions, with the T7 promoter  
337 containing annealed oligonucleotides. Reactions were incubated for 16h at 37°C, DNase (NEB)  
338 digested and purified using the RNA Clean & Concentrator-25 kit (ZymoResearch, Irvine, USA).

339 **RPA primer and crRNA design.** Genetically conserved regions in the BKV and CMV genome  
340 were identified using publicly accessible databases (Virus Pathogen Resource and NCBI).  
341 Alignments were performed using MAFFT<sup>32</sup> and visualized with Jalview<sup>33</sup>. RPA primer design

342 was done using NCBI's PRIMER-BLAST tool with previously described settings<sup>3</sup>. *CXCL9* RPA  
343 primers were designed to be in proximity to previously published qPCR primers<sup>18</sup>. For each  
344 region to be amplified, optimal primer pairs were identified by forward and reverse primer  
345 screens. Primer concentrations were optimized by testing different forward and reverse primer  
346 concentrations in a dilution matrix. crRNAs, 28 nucleotides complementary to the target region,  
347 were designed as previously described<sup>1,3</sup> and tested for their performance with each RPA  
348 primer pair. The sequences, including spacer, direct repeat and T7 promoter, are indicated in  
349 Supplementary Table 4.

350 **qRT-PCR.** RNA isolation, reverse transcription and qPCR were performed as previously  
351 described<sup>18</sup>. Briefly, we reverse transcribed RNA using the TaqMan Reverse Transcription kit  
352 (ThermoFisher, Waltham, USA) with random hexamers. The qPCR was performed using cDNA  
353 without pre-amplification. qPCR reactions were set up as previously described<sup>18</sup>. All reactions  
354 were performed in duplicate, using the Applied Biosystems StepOne Plus real-time PCR system  
355 (ThermoFisher, Waltham, USA). In-vitro transcribed RNA for *CXCL9* served as a standard  
356 (sequences in Supplementary Table 4). For expression analysis, we employed the comparative  
357  $C_T$  method<sup>34</sup> for relative quantification to 18S RNA (Supplementary Figure 3a) or used absolute  
358 quantification based on a *CXCL9* standard curve (Figures 5b,c). Expression levels are  
359 presented on a logarithmic scale relative to the control, whose average expression was set to 1.

360 **RPA reactions.** For RPA reactions, the TwistAmp Liquid Basic kit (TwistDx Limited,  
361 Maidenhead, UK) was used according to the manufacturer's instructions with the following  
362 modifications. Primer concentrations were 120nM for the forward primer and 480nM for the  
363 reverse primer. The total reaction volume was 20 $\mu$ l with a final concentration of dNTPs at  
364 7.2mM (each) and MgOAc at 8mM. RPA reactions were incubated at 37°C for 50min. For rt-  
365 RPA reactions, forward and reverse primers were used at 480nM each and MgOAc at 14mM.  
366 1 $\mu$ l GoScript reverse transcriptase (Promega) was added to a 20 $\mu$ l reaction containing DL-  
367 Dithiothreitol solution (DTT, Sigma-Aldrich) at a final concentration of 19mM. The primer-RNA  
368 mix was pre-incubated at 65°C for 10min and the rt-RPA reaction was performed at 42°C for  
369 60min.

370 **Cas13 reactions.** Detection of (rt)RPA amplified targets was performed as described  
371 previously<sup>1-3</sup> with minor modifications. NEB buffer 2 (NEB, Ipswich, USA) served as cleavage  
372 buffer at a final concentration of 1X. 3 $\mu$ l of RPA or rtRPA product were used in a 20 $\mu$ l Cas13  
373 reaction. Fluorescence (485nm excitation, 520nm emission) was measured on a plate reader  
374 (SpectraMax M5, Molecular Devices, San Jose, USA) every 5min for up to 3h at 37°C.

375 **One-pot reaction.** One pot RPA-CRISPR reactions were performed with murine RNase  
376 Inhibitor (NEB) at 1U/μl, Cas13 at 45nM, crRNA at 22.5nM, RNase Alert V2 (Thermofisher) at  
377 125nM, human background RNA (from 293T cells) at 1.25ng/μl, T7 polymerase (Lucigen) at  
378 0.6μl/20μl, dNTPs at 1.8mM (each), rNTPs at 0.5mM (each), MgOAc at 16mM and the buffers  
379 of the RPA TwistAmp Liquid Basic kit (2X, 10X and 20X buffers) at 1X final concentrations.

380 **Diagnostic BKV and CMV quantitative PCR.** De-identified patient samples were provided by  
381 the Crimson Core at Brigham and Women's Hospital. Quantification of BKV and CMV viral load  
382 were performed at the CLIA certified diagnostic core facility at Brigham and Women's  
383 Hospital. In brief, BKV viral load samples were processed using the Luminex Aries instrument  
384 (Luminex, Austin, USA) and a laboratory-developed protocol for a probe-free, two-primer, real-  
385 time PCR system. Following amplification, a thermal melt was performed. The system software  
386 allows for a quantitation template, developed using a standard curve calibrated against the 1<sup>st</sup>  
387 WHO International Standard for BKV, to be applied to raw data for production of a quantitative  
388 value, reported in copies/mL (C/mL). CMV viral load samples were processed using the Roche  
389 Cobas AmpliPrep/Cobas TaqMan CMV Test (IVD) on the Roche-docked Cobas  
390 AmpliPrep/TaqMan instrument. This is a real time PCR system that automates specimen  
391 preparation, PCR amplification, target detection and quantitation. Results are reported in  
392 International Units/mL (IU/mL).

393 **Patient populations.** For the CMV and BK studies, de-identified samples collected for clinical  
394 testing for CMV and BK viremia at the Brigham and Women's Hospital (BWH) were provided by  
395 the Crimson Core at BWH. Clinical reported results for CMV and BK viremia were then  
396 compared to CRISPR/Cas13 diagnostics results. For the rejection and BK nephropathy  
397 samples, patients were recruited prior to a kidney transplant biopsy to investigate an elevation  
398 of creatinine at BWH. Prospective sample collection was also performed in few kidney  
399 transplant recipients starting in January 2019 until June 2019. Samples started to be collected  
400 after one month of transplantation to avoid the impact of surgery and ischemic time. Samples  
401 were then collected according to clinical visits for 3-5 collections within the first year of  
402 transplant. The kidney transplant cohort is representative of kidney transplant recipients in this  
403 geographical location and at a tertiary academic hospital.

404 **Study design and participants.** The study was approved by the Institutional Review Board at  
405 Brigham and Women's Hospital (2017P000298), and the procedures followed were in  
406 accordance with institutional guidelines. In this observational study, a total of 31 kidney  
407 transplant patients were enrolled, and informed consent was obtained from all subjects  
408 (Supplementary Tables 1,2). Urine samples were collected from patients undergoing kidney

409 biopsy for clinical indications. The cohort of samples was then selected based on the presence  
410 of cellular rejection or no rejection on biopsy findings. For the prospective analyzes, samples  
411 were provided by a cohort from Montefiore Medical Center, Bronx, NY (Montefiore/Einstein  
412 Institutional Review Board (09-06-174). Briefly, longitudinal samples were collected at the  
413 following time points: 0-3 months, 6-9 months and 9-12 months post-transplant or when clinical  
414 biopsy was performed). Selection of patients was based on availability of at least three samples  
415 collected either before or after rejection event that was classified as rejection Banff IA or higher.  
416 **Ethics statement.** We have complied with all relevant ethical regulations. The patient samples  
417 used in this study were obtained from the clinical study “*Biomarkers in Kidney Transplantation*”  
418 which was approved by Partners Human Research Committee (2017P000298/PHS). We have  
419 obtained written informed consent from all participants.

420 **Data availability statement.** The authors declare that the data supporting the findings of this  
421 study are available within the paper and its supplementary information files.

422 **Code availability statement.** The lateral flow quantification app code is available at  
423 [https://github.com/jackievaleri/lateral\\_flow\\_quantification\\_app](https://github.com/jackievaleri/lateral_flow_quantification_app).

424

## 425 **References**

- 426 1. Gootenberg, J. S. *et al.* Nucleic acid detection with CRISPR-Cas13a/C2c2. *Science (80- )*. **356**,  
427 438–442 (2017).
- 428 2. Myhrvold, C. *et al.* Field-deployable viral diagnostics using CRISPR-Cas13. *Science (80- )*. **448**,  
429 444–448 (2018).
- 430 3. Gootenberg, J. S. *et al.* Multiplexed and portable nucleic acid detection platform with Cas13,  
431 Cas12a, and Csm6. *Science (80- )*. **0179**, (2018).
- 432 4. Chen, J. S. *et al.* CRISPR-Cas12a target binding unleashes indiscriminate single-stranded DNase  
433 activity. *Science* **360**, 436–439 (2018).
- 434 5. Harrington, L. B. *et al.* Programmed DNA destruction by miniature CRISPR-Cas14 enzymes.  
435 *Science (80- )*. **362**, 839 LP – 842 (2018).
- 436 6. Pardee, K. *et al.* Rapid, Low-Cost Detection of Zika Virus Using Programmable Biomolecular  
437 Components. *Cell* **165**, 1255–1266 (2016).
- 438 7. Hajian, R. *et al.* Detection of unamplified target genes via CRISPR–Cas9 immobilized on a  
439 graphene field-effect transistor. *Nat. Biomed. Eng.* **3**, (2019).
- 440 8. Wu, Y., Liu, S.-X., Wang, F. & Zeng, M.-S. Room Temperature Detection of Plasma Epstein–Barr  
441 Virus DNA with CRISPR–Cas13. *Clin. Chem.* **65**, 591 LP – 592 (2019).
- 442 9. Lamb, K. E., Lodhi, S. & Meier-Kriesche, H.-U. Long-Term Renal Allograft Survival in the United  
443 States: A Critical Reappraisal. *Am. J. Transplant.* **11**, 450–462 (2011).
- 444 10. Tullius, S. G. & Rabb, H. Improving the Supply and Quality of Deceased-Donor Organs for

- 445 Transplantation. *N. Engl. J. Med.* **378**, 1920–1929 (2018).
- 446 11. Wekerle, T., Segev, D., Lechler, R. & Oberbauer, R. Strategies for long-term preservation of  
447 kidney graft function. *Lancet* **389**, 2152–2162 (2017).
- 448 12. Ross, S. A., Novak, Z., Pati, S. & Boppana, S. B. Overview of the diagnosis of cytomegalovirus  
449 infection. *Infect. Disord. Drug Targets* **11**, 466–474 (2011).
- 450 13. Randhawa, P. *et al.* Correlates of quantitative measurement of BK polyomavirus (BKV) DNA with  
451 clinical course of BKV infection in renal transplant patients. *J. Clin. Microbiol.* **42**, 1176–1180  
452 (2004).
- 453 14. Fishman, J. A. Infection in Organ Transplantation. *Am. J. Transplant.* **17**, 856–879 (2017).
- 454 15. Sepkowitz, K. A. Opportunistic Infections in Patients with and Patients without Acquired  
455 Immunodeficiency Syndrome. *Clin. Infect. Dis.* **34**, 1098–1107 (2002).
- 456 16. Sundsfjord, A. *et al.* BK and JC Viruses in Human Immunodeficiency Virus Type 1-Infected  
457 Persons: Prevalence, Excretion, Viremia, and Viral Regulatory Regions. *J. Infect. Dis.* **169**, 485–  
458 490 (1994).
- 459 17. Jackson, J. A. *et al.* Urinary chemokines CXCL9 and CXCL10 are noninvasive markers of renal  
460 allograft rejection and BK viral infection. *Am. J. Transplant.* **11**, 2228–2234 (2011).
- 461 18. Hricik, D. E. *et al.* Multicenter validation of urinary CXCL9 as a risk-stratifying biomarker for kidney  
462 transplant injury. *Am. J. Transplant.* (2013) doi:10.1111/ajt.12426.
- 463 19. Schaub, S. *et al.* Urinary CXCL9 and CXCL10 levels correlate with the extent of subclinical  
464 tubulitis. *Am. J. Transplant.* **9**, 1347–1353 (2009).
- 465 20. Rabant, M. *et al.* Early Low Urinary CXCL9 and CXCL10 Might Predict Immunological Quiescence  
466 in Clinically and Histologically Stable Kidney Recipients. *Am. J. Transplant.* **16**, 1868–1881 (2016).
- 467 21. Fishman, J. A. Infection in Solid-Organ Transplant Recipients. *N. Engl. J. Med.* **357**, 2601–2614  
468 (2007).
- 469 22. El-Zoghby, Z. M. *et al.* Identifying specific causes of kidney allograft loss. *Am. J. Transplant* **9**,  
470 527–535 (2009).
- 471 23. Henderson, L. K., Nankivell, B. J. & Chapman, J. R. Surveillance protocol kidney transplant  
472 biopsies: their evolving role in clinical practice. *Am. J. Transplant* **11**, 1570–1575 (2011).
- 473 24. Parajuli, S. *et al.* Donor-Specific Antibodies in the Absence of Rejection Are Not a Risk Factor for  
474 Allograft Failure. *Kidney Int. reports* **4**, 1057–1065 (2019).
- 475 25. Schinstock, C. A. *et al.* The Value of Protocol Biopsies to Identify Patients With De Novo Donor-  
476 Specific Antibody at High Risk for Allograft Loss. *Am. J. Transplant* **17**, 1574–1584 (2017).
- 477 26. Bloom, R. D. *et al.* Cell-Free DNA and Active Rejection in Kidney Allografts. *J. Am. Soc. Nephrol.*  
478 **28**, 2221–2232 (2017).
- 479 27. Sigdel, T. K. *et al.* Optimizing Detection of Kidney Transplant Injury by Assessment of Donor-  
480 Derived Cell-Free DNA via Massively Multiplex PCR. *J. Clin. Med.* **8**, (2018).
- 481 28. UNITED STATES SECURITIES AND EXCHANGE COMMISSION.

- 482 <https://www.sec.gov/Archives/edgar/data/1217234/000156459018006584/cdna->  
483 [10k\\_20171231.htm](https://www.sec.gov/Archives/edgar/data/1217234/000156459018006584/cdna-10k_20171231.htm).
- 484 29. Hricik, D. E. *et al.* Adverse Outcomes of Tacrolimus Withdrawal in Immune–Quiescent Kidney  
485 Transplant Recipients. *J. Am. Soc. Nephrol.* **26**, 3114–3122 (2015).
- 486 30. Curtis, K. A. *et al.* Isothermal Amplification Using a Chemical Heating Device for Point-of-Care  
487 Detection of HIV-1. *PLoS One* **7**, e31432 (2012).
- 488 31. Ahn, M.-H., Baek, S.-K., Min, J. & Park, J.-H. A portable electromagnetic induction heating device  
489 for point-of-care diagnostics. *BioChip J.* **10**, 208–214 (2016).
- 490 32. Katoh, K. & Standley, D. M. MAFFT multiple sequence alignment software version 7:  
491 improvements in performance and usability. *Mol. Biol. Evol.* **30**, 772–780 (2013).
- 492 33. Waterhouse, A. M., Procter, J. B., Martin, D. M. A., Clamp, M. & Barton, G. J. Jalview Version 2—  
493 a multiple sequence alignment editor and analysis workbench. *Bioinformatics* **25**, 1189–1191  
494 (2009).
- 495 34. Schmittgen, T. D. & Livak, K. J. Analyzing real-time PCR data by the comparative CT method. *Nat.*  
496 *Protoc.* **3**, 1101 (2008).

497

#### 498 **Acknowledgments**

499 We thank Rebecca Zaffini from viral microbiology (Brigham & Women’s Hospital) for helpful  
500 discussion about BKV testing and qPCR. We thank the Crimson Core at Brigham & Women’s  
501 Hospital for providing CMV and BKV patient samples. M.M.K was supported by the German  
502 Academy of Sciences, Leopoldina (LPDS 2018-01) and the Clinician Scientist Program Berta-  
503 Ottenstein of the Faculty of Medicine, University of Freiburg, Germany. M.A.A was supported  
504 by a National Science Foundation graduate research fellowship (1122374). V.K. was  
505 supported by the DFG (403877094). J.J.C. was supported by MIT’s Center for Microbiome  
506 Informatics and Therapeutics, the Paul G. Allen Frontiers Group, and the Wyss Institute. We  
507 thank Helena de Puig, Nicolaas Angenent-Mari, Aaron Dy and Xiao Tan for helpful discussions.

508

#### 509 **Author contributions**

510 M.M.K., L.V.R. and J.J.C. designed the study. M.M.K., M.A.A., A.C.H., I.L. and R.G. performed  
511 experiments. J.V. and M.A.A. programmed the smartphone app, L.V.R. provided clinical  
512 samples. All authors contributed to the writing of the manuscript and interpretation of data.

513

#### 514 **Competing interests**

515 A patent application is pending. J.J.C is co-founder and director of Sherlock Biosciences.



**Figure 1**

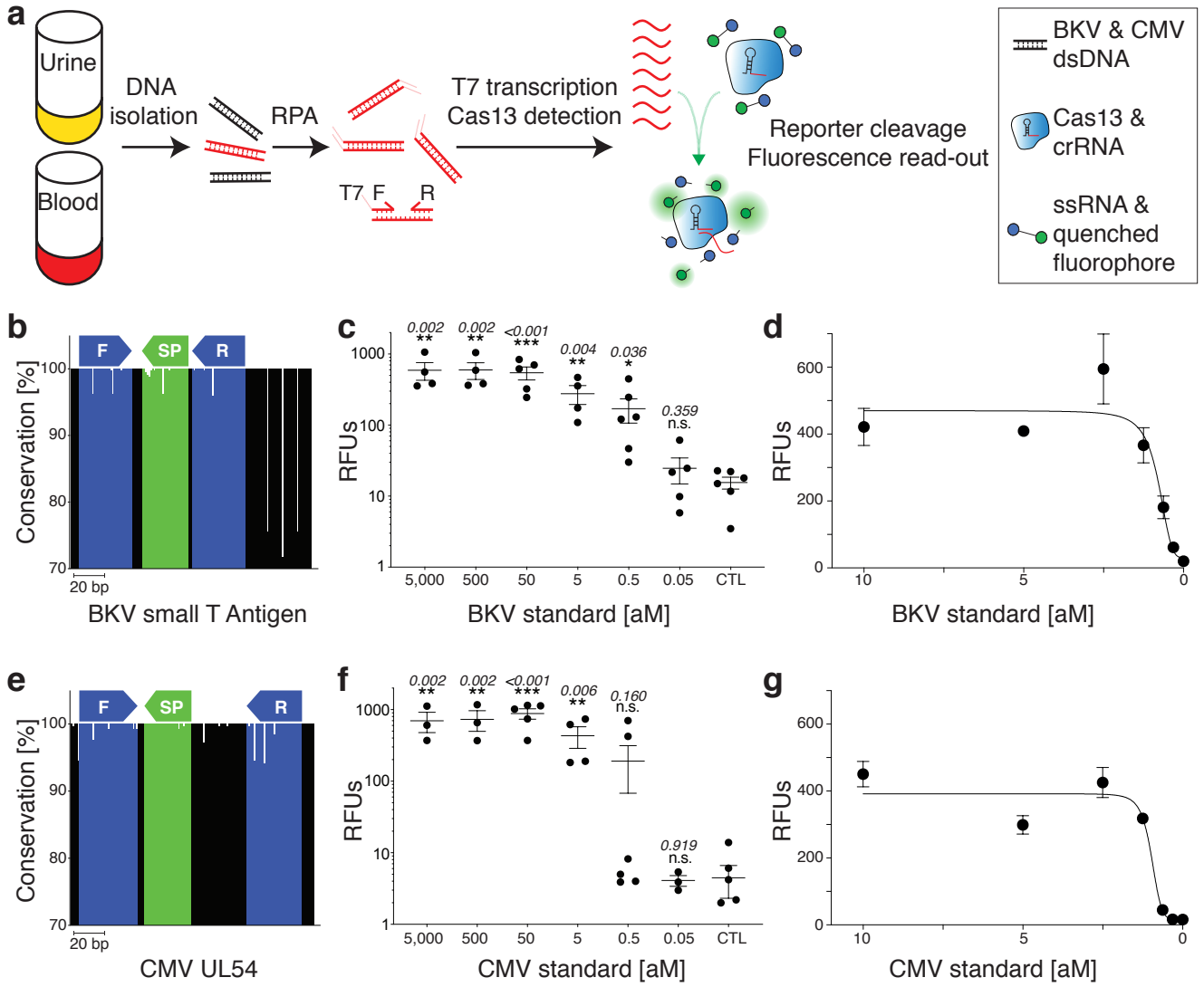
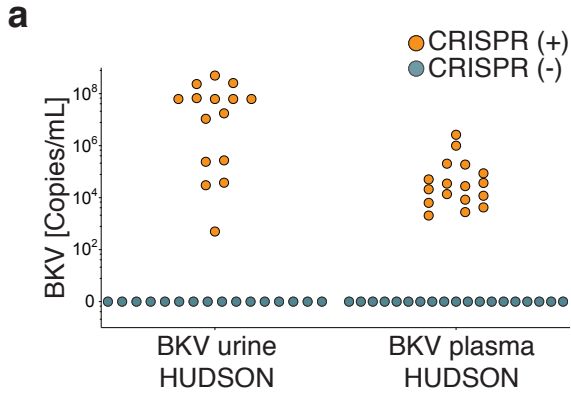


**Figure 2**

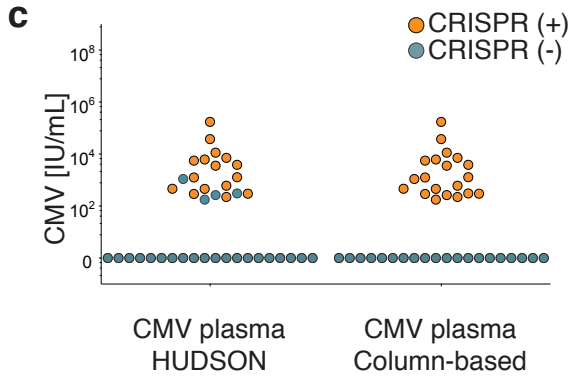


**b**

	VIRUS (+)	VIRUS (-)
CRISPR (+)	<b>True positive</b>	False positive
CRISPR (-)	False negative	<b>True negative</b>

*Sensitivity      Specificity*

BKV urine HUDSON	BKV plasma HUDSON
15    0	17    0
0    16	0    19
100% 100%	100% 100%



**d**

CMV plasma HUDSON	CMV plasma column-based
16    0	20    0
4    20	0    20
80% 100%	100% 100%

**Figure 3**

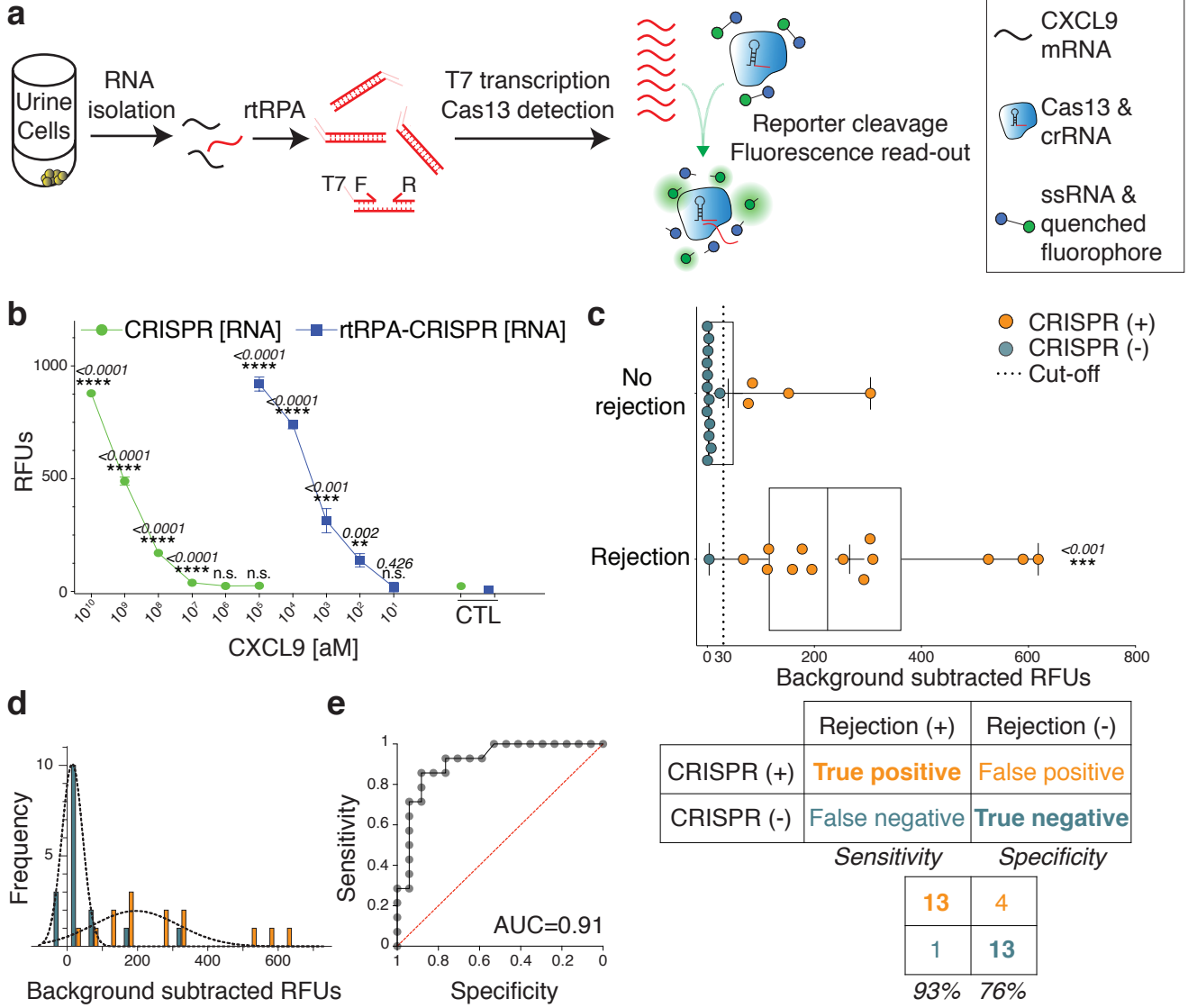


**Figure 4**

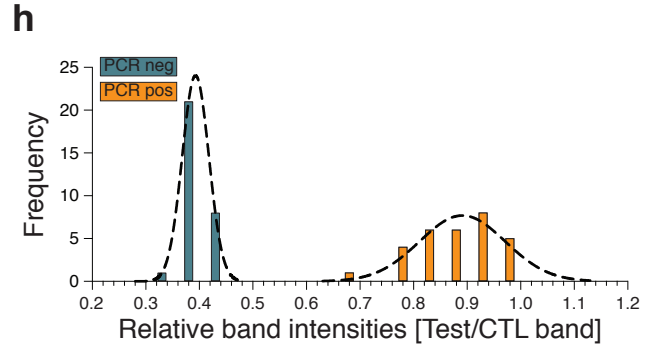
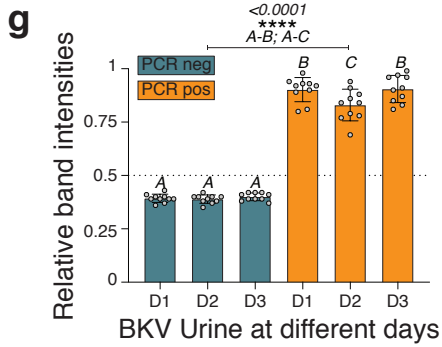
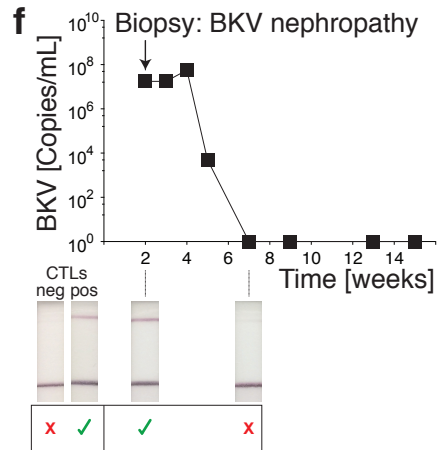
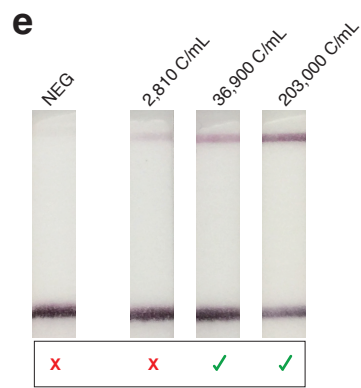
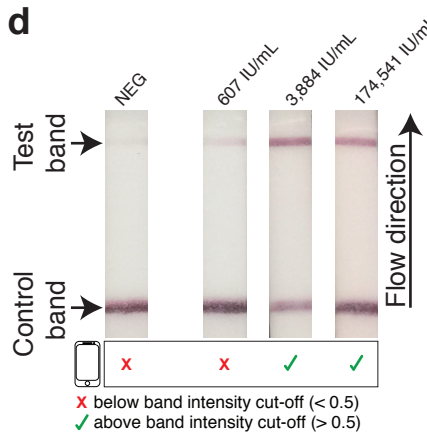
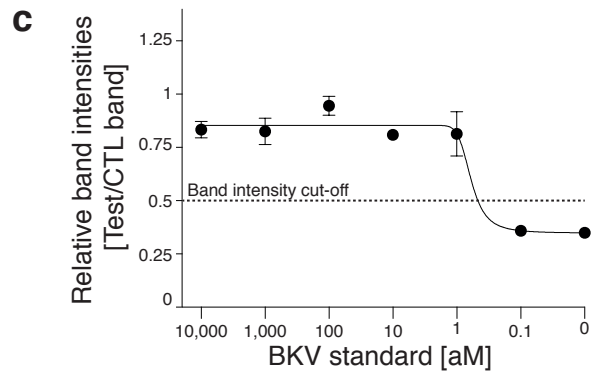
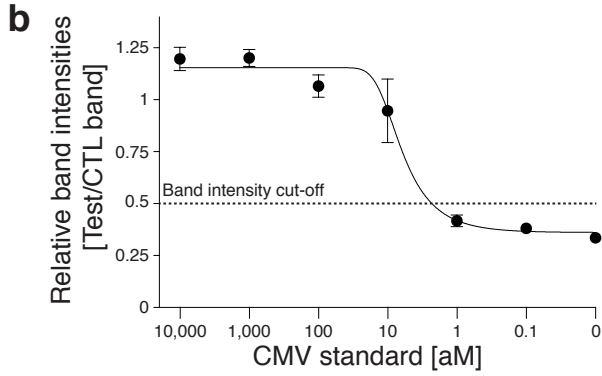
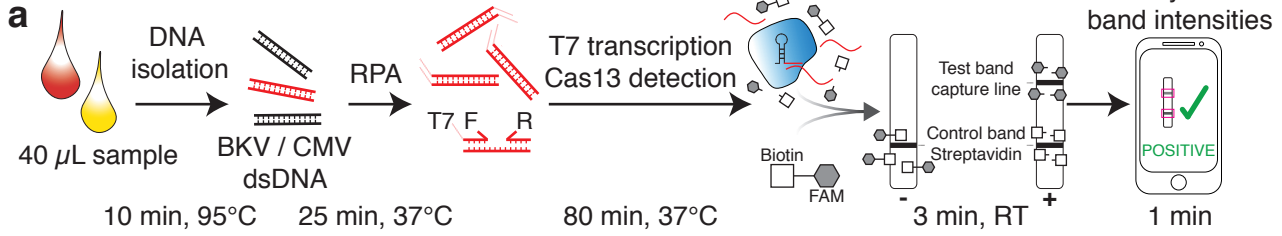
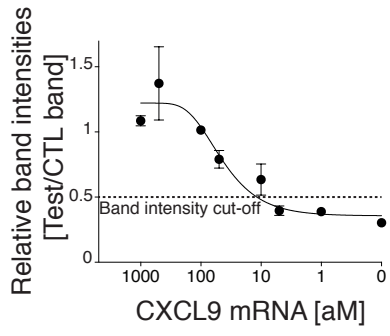
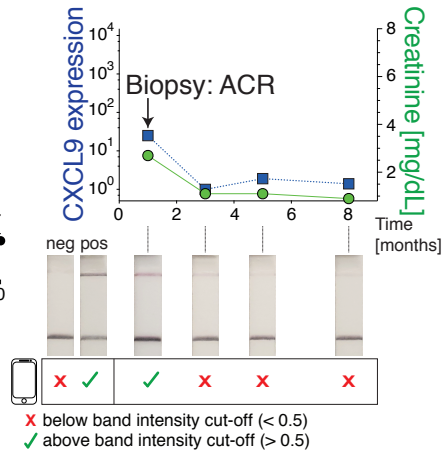


**Figure 5**

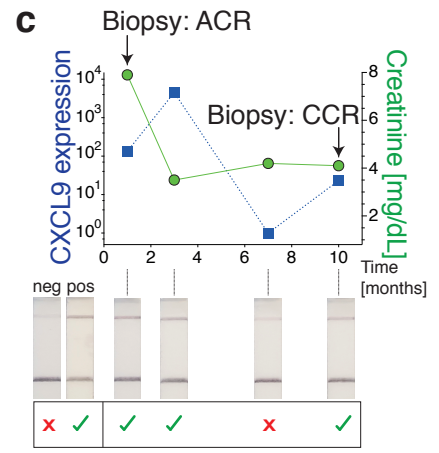
**a**



**b**



**c**

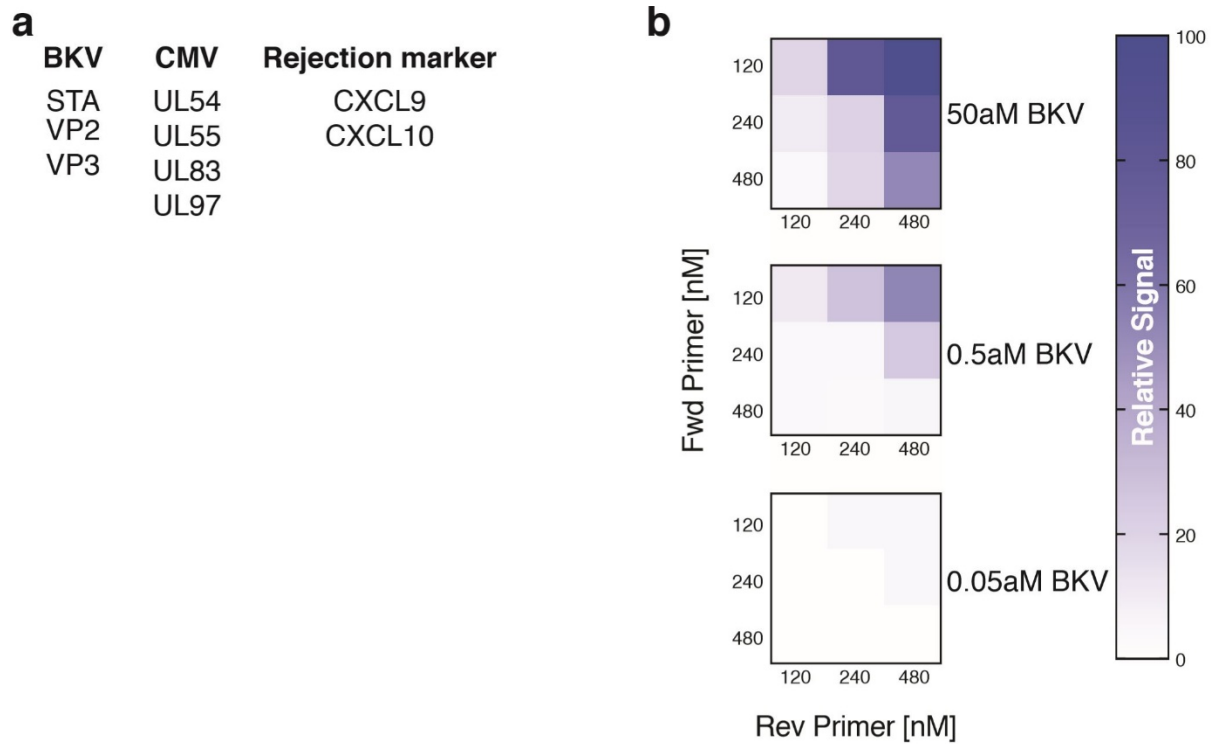


## **Supplementary Information**

### **Contents:**

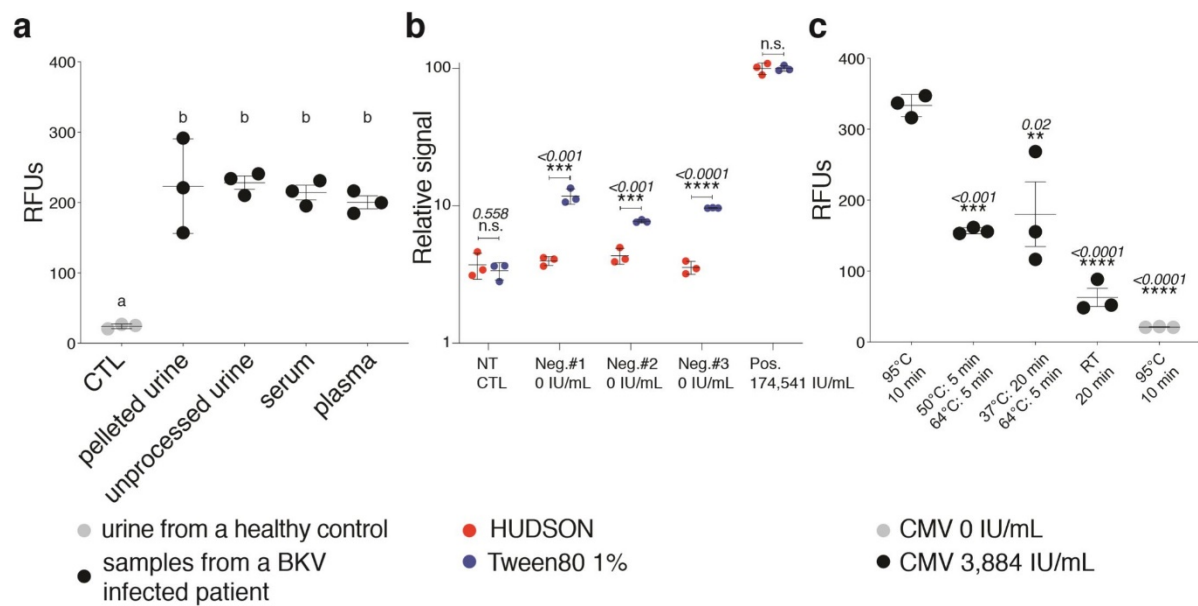
- Supplementary Figures 1-5
- Supplementary Tables 1-4

## Figure S1



**Supplementary Figure 1 Target genes and primer optimization.** **a**, Target genes tested for detection of BKV or CMV infection and rejection. **b**, RPA primer dilution matrix. The Sherlock fluorescence signal of BKV detection (ATCC synthetic standard) at the indicated target concentrations is depicted as colour intensity relative to the highest signal (100). Forward and reverse primer concentrations for RPA as indicated.

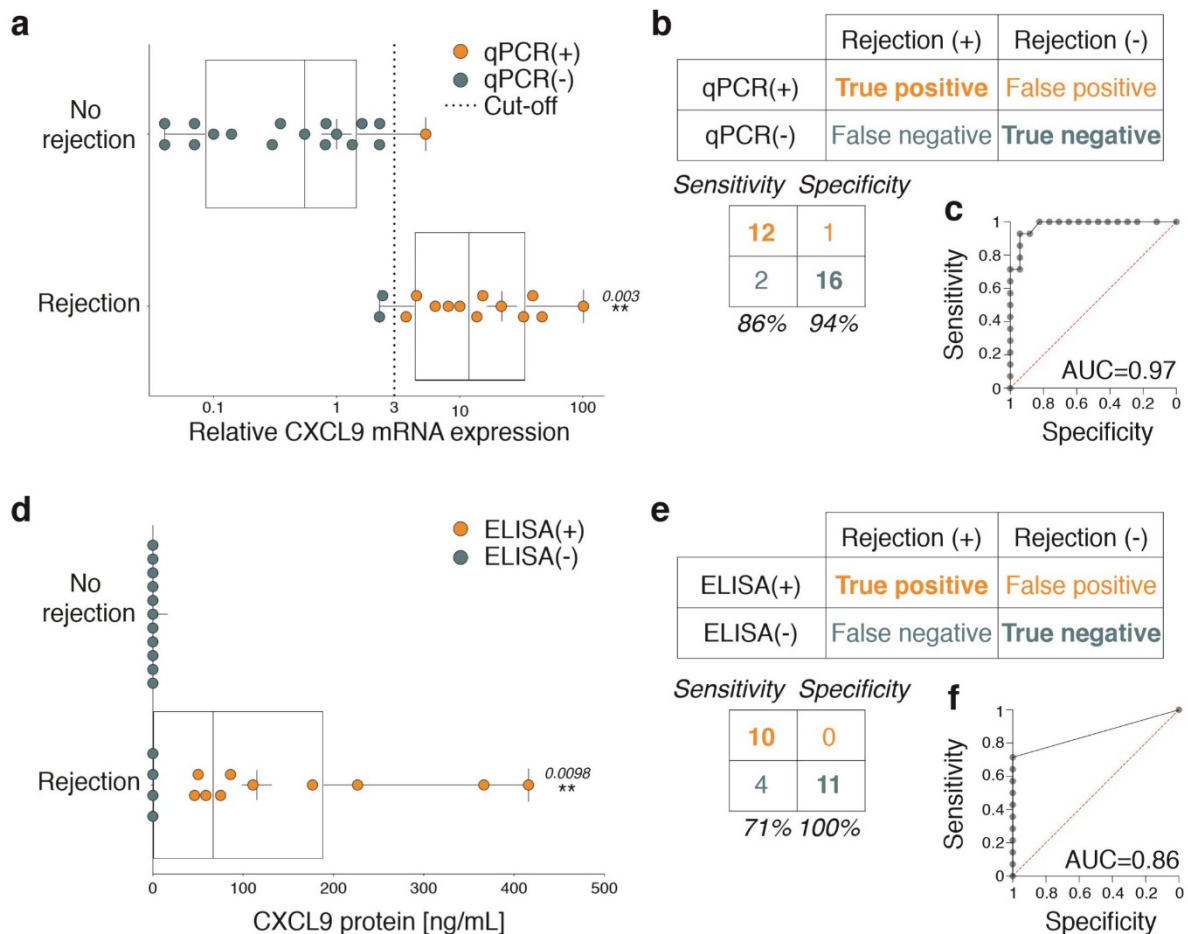
**Figure S2**



**Supplementary Figure 2 Comparison of different specimen types and sample processing.** **a**, Detection of BKV in the indicated specimens from the same patient compared to urine from a healthy control. Different small letters indicate significant differences as assessed by one-way ANOVA and Tukey's multiple comparisons test. Symbols: mean  $\pm$  SD of 3 independent reactions. **b**, Comparison of sample processing by the HUDSON method (red circles) and incubation with Tween80 1% for 20 min at room temperature (blue circles). Tested on 3 different CMV negative patient samples to test for unspecific background noise and one CMV positive patient sample. Fluorescence was normalized to the highest signal (HUDSON, 100). Asterisks indicate significant differences as assessed by Student's two-tailed t-test. Symbols: mean  $\pm$  SD of 3 independent reactions. **c**, Comparison of different HUDSON-based protocols on a CMV negative (grey circles) and a CMV positive (black circles) patient sample. Asterisks indicate significant differences to the 95°C/10 min (3884 IU/mL) condition as assessed by one-way ANOVA and Dunnett's multiple comparisons test. Symbols: mean  $\pm$  SD of 3 independent reactions. n.s. not significant,  $p < 0.05$  (\*),  $p < 0.01$  (\*\*),  $p < 0.001$  (\*\*\*),  $p < 0.0001$  (\*\*\*\*) (**b,c**).



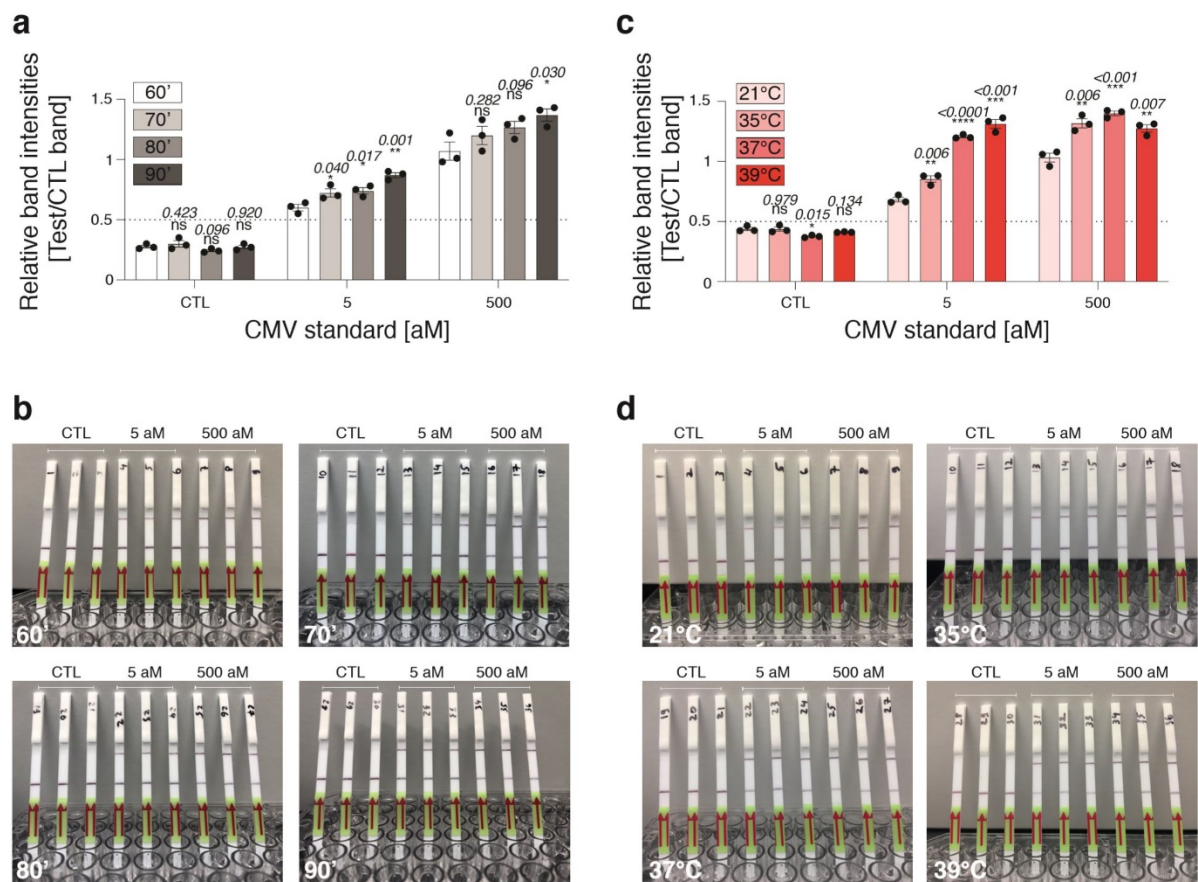
**Figure S3**



**Supplementary Figure 3 CXCL9 mRNA and protein levels in rejection patients and controls.** **a**, qPCR-based detection of CXCL9 mRNA in rejection patients (n=14) and no rejection control patients (n=17). Blue circles indicate qPCR negative tests and orange circles indicate qPCR positive test results. The dashed line indicates the cut-off differentiating between a negative and positive test result. **b**, Sensitivity and specificity of rejection detection by qPCR calculated using the cut-off value depicted in (a). **c**, Area under the receiver-operating-characteristic (ROC) curve (AUC) assessing the accuracy of qPCR-based rejection diagnostics (1 indicates perfect discriminatory value; 0.5 or less indicates no discriminatory value). **d**, ELISA-based detection of CXCL9 protein in rejection patients (n=14) and no rejection control patients (n=11). The tested samples were the same as depicted in (a) (rejection) or a subset of them (no rejection). Blue circles indicate ELISA negative tests and orange circles indicate ELISA positive test results. **e**, Confusion matrix indicating the sensitivity and specificity of ELISA-based rejection detection. **f**, Area under the receiver-operating-characteristic (ROC) curve (AUC) assessing the accuracy of ELISA-based rejection diagnostics (1 indicates perfect discriminatory value; 0.5 or less indicates no discriminatory value).

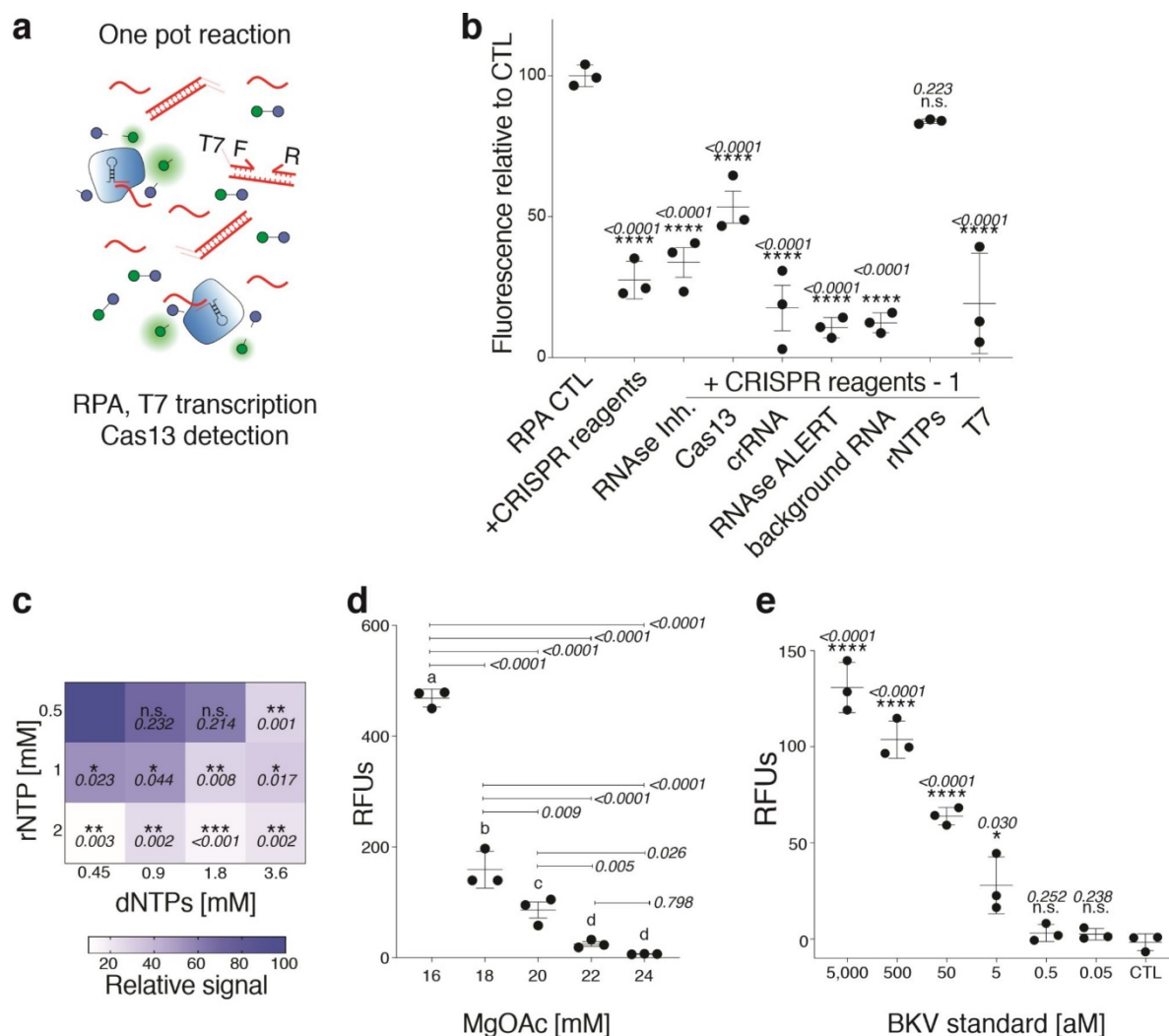
Box plot lines: median and quartiles, whiskers: data range, crosses: averages. Each symbol represents a different, independent patient sample. Asterisks: significant difference to control as assessed by Student's two-tailed t-test.  $p < 0.01$  (\*\*) (a,d)

**Figure S4**



**Supplementary Figure 4 Influence of temperature and incubation time on lateral-flow band intensity.** **a**, Incubation of the CRISPR reaction detecting the CMV synthetic standard at the indicated concentrations for the indicated reaction times. The lateral-flow-based readout was quantified as the ratio of test/control band. The dashed line indicates the assay's cut-off. Symbols: mean  $\pm$  SD of 3 independent reactions. Asterisks indicate significant differences to the 60 min control reaction time as assessed by Student's two-tailed t-test. **b**, Images of the lateral-flow assays quantified in (a). **c**, Incubation at different temperatures for the detection of the CMV synthetic standard at the indicated concentrations with lateral flow. Symbols: mean  $\pm$  SD of 3 independent reactions. Asterisks indicate significant differences to the 21°C control reaction as assessed by Student's two-tailed t-test. **d**, Images of the lateral-flow assays quantified in (c). n.s. not significant,  $p < 0.05$  (\*),  $p < 0.01$  (\*\*),  $p < 0.001$  (\*\*\*),  $p < 0.0001$  (\*\*\*\*).

**Figure S5**



**Supplementary Figure 5 Optimization of the one-pot reaction.** **a**, Schematic illustration of the one-pot assay. **b**, Effect of CRISPR and T7 transcription reagents upon addition to the RPA reaction. CRISPR reagents were added pooled (+CRISPR reagents) or as a pool with one component missing (+CRISPR reagents -1). CMV synthetic DNA served as target (500aM). A separate CRISPR/T7 reaction served as readout. Fluorescence was normalized to the highest signal (RPA CTL, 100). Asterisks indicate significant differences to the RPA control without any additions (RPA CTL) as assessed by one-way ANOVA and Dunnett's multiple comparisons test. Symbols: mean  $\pm$  SD of 3 independent reactions. **c**, Concentration matrix of rNTPs and dNTPs in the one-pot reaction. The fluorescence signal is depicted as colour intensity relative to the highest signal. Asterisks indicate significant differences as assessed by Student's two-tailed t-test. **d**, Testing of the indicated MgOAc concentrations in the one-pot reaction. CMV synthetic DNA served as target (500aM). Different letters indicate significant differences between groups as assessed by one-way ANOVA and Tukey's multiple comparisons test. Symbols: mean  $\pm$  SD of 3 independent reactions. **e**, One-pot reaction detecting the ATCC quantitative BKV synthetic standard (Dunlop strain) at the indicated concentrations. Symbols: mean  $\pm$  SD of 3 independent reactions. Asterisks indicate significant differences to no template control (CTL) as assessed by Student's two-tailed t-test.  $p < 0.05$  (\*),  $p < 0.01$  (\*\*),  $p < 0.001$  (\*\*\*),  $p < 0.0001$  (\*\*\*\*).

**Table S1**

Characteristics	All subjects (N=31)	Rejection (n=14)	No Rejection (n=17)	p-value
Recipient Age (years)				
Mean $\pm$ SD	59 $\pm$ 13	61 $\pm$ 12	57 $\pm$ 14	0.589
Recipient Gender				
Female (n, %)	17 (54.8%)	5 (35.7%)	12 (70.6%)	0.076
Male (n, %)	14 (45.2%)	9 (64.3%)	5 (29.4%)	
Recipient Race				
African American (n, %)	10 (32.2%)	7 (50.0%)	3 (17.6%)	0.131
Caucasian (n, %)	14 (45.1%)	4 (28.6%)	10 (58.8%)	
Other / Unknown	7 (22.6%)	3 (21.4%)	4 (23.6%)	
Donor gender				
Female (n, %)	20 (64.5%)	9 (64.3%)	11 (64.7%)	0.999
Male (n, %)	11 (35.5%)	5 (35.7%)	6 (83.3%)	
Donor Source				
Living (n, %)	11 (35.5%)	4 (28.6%)	7 (41.2%)	0.707
Deceased (n, %)	20 (64.5%)	10 (71.4%)	10 (58.8%)	
Number of HLA mismatches				
Mean $\pm$ SD	4.4 $\pm$ 1.2	4.2 $\pm$ 0.9	4.6 $\pm$ 1.4	0.096
Induction Therapy				
Thymoglobulin (n, %)	16 (51.6%)	5 (35.7%)	11 (64.7%)	0.268
Basiliximab (n, %)	14 (45.2%)	8 (57.1%)	6 (35.3%)	
Alemtuzumab (n, %)	1 (3.2%)	1 (7.2%)	0 (0.0%)	
Time since transplant (months)				
Mean $\pm$ SD	12 $\pm$ 12	14 $\pm$ 13	11 $\pm$ 12	0.256
Cause of kidney disease				
Diabetes	7 (22.6%)	4 (28.5%)	3 (17.6%)	0.464
Polycystic kidney disease	5 (16.2%)	3 (21.5%)	2 (11.8%)	
Glomerulopathy	8 (25.8%)	3 (21.5%)	5 (29.5%)	
Interstitial Nephritis	3 (9.6%)	0 (0.0%)	3 (17.6%)	
Other/Unknown	8 (25.8%)	4 (28.5%)	4 (23.5%)	

**Supplementary Table 1. Baseline and demographic characteristics of kidney transplanted patients.** Baseline characteristics are presented as mean  $\pm$  SD. For non-categorical variables, data were analysed using Mann-Whitney test. For categorical variables, data were analysed using Fisher's exact test.

**Table S2**

<b>Characteristics</b>	<b>n=14</b>
Creatinine (mg/dL)	3.24 ± 1.63
eGFR (ml/min/1.73m <sup>2</sup> )	23.21 ± 9.27
Rejection Type (n, %)	
Borderline	1 (7.2%)
IA/IB	8 (57.1%)
IIA/IIB	4 (28.5%)
III	1 (7.2%)
Banff g score	1.5 ± 1.4
Banff i score	2.4 ± 0.8
Banff t score	2.1 ± 0.8
Banff v score	0.6 ± 0.9
Banff ptc score	1.5 ± 1.3
Banff ci score	1.2 ± 0.7
Banff ct score	1.2 ± 1.0
Banff cv score	1.2 ± 1.0
Banff cg score	0.6 ± 0.9
Banff ah score	0.6 ± 0.9
C4d score	0.6 ± 1.2

**Supplementary Table 2. Diagnosis at the time of biopsy from rejection patients' cohort.** Data is expressed as mean ± SD. Banff score abbreviations: glomerulitis (g), interstitial inflammation (i), tubulitis (t), intimal arteritis (v) peritubular capillaritis (ptc), interstitial fibrosis (ci), tubular atrophy (ct), vascular fibrous intimal thickening (cv), glomerular basement membrane double contours (cg), arteriolar hyalinosis (ah).

**Table S3**

	<b>ELISA</b>	<b>Biolayer interferometry</b>	<b>CRISPR diagnostics</b>	<b>qPCR</b>
<b>Reference</b>	RND systems (DCX900) Hricik et al., 2013	Gandolfini et al., 2017	this paper	Altona diagnostics, RealStar Kits 021003 (CMV); 031003 (BKV)
<b>Analyte</b>	CXCL9 protein	CXCL9 protein	CXCL9 mRNA; BKV & CMV DNA	BKV & CMV DNA
<b>Speed</b>				
Assay length	4h 30min	60min	108min	85min
Hands-on time	1h 20min	10min	10min	10min
<b>Costs</b>				
Equipment	> \$5,000 USD	> \$100,000 USD (OctetRED96)	> \$5,000 USD (fluorescence) \$2.3 USD per test (lateral flow)	> \$5,000 USD
Reagents (per test)	\$5.4 USD	\$1 USD	\$1 USD	\$20 USD
<b>Sensitivity</b>	11.3 pg/mL	35 pg/mL	low attomolar range	low attomolar range
<b>POCT compatibility</b>				
Isothermal incubation	Yes	Yes	Yes	No
Minimal equipment	No	No	Yes (lateral flow)	No
Visual output	No	No	Yes (lateral flow)	No

**Supplementary Table 3.** Comparison of CRISPR diagnostics with ELISA, biolayer interferometry and qPCR for the detection of CXCL9, BKV and CMV.

**Table S4**

Name	Sequence (5' – 3')
<b>RPA Primer</b>	
BKV_STA_fwd	GAAATTAATACGACTCACTATAGGCATTGCAGAGTTCTTCAGTTAGGTCTAAGCC
BKV_STA_rev	AATTTTTAAGAAAAGAGCCCTTGGTTTGGATA
CMV_UL54_fwd	GAAATTAATACGACTCACTATAGGGCACCAGCCGAACGTGGTGATCCGCCGATCGATGAC
CMV_UL54_rev	CTATCAGCAACTGGACCATGGCCAGAAAAATCG
CXCL9_fwd	GAAATTAATACGACTCACTATAGGTATCCACCTACAATCCTTGAAAGACCTTAAAC
CXCL9_rev	TTAGACATGTTTGAACCTCATTCTTCAGTGTA
<b>qPCR Primer and Probes</b>	
CXCL9_fwd	CTTTTCCTCTTGGGCATCATCT
CXCL9_rev	AGGAACAGCGACCCTTTCTCA
CXCL9 probe	FAM-TACTGGGGTTCCTTGCCTCAATCAGA-TAMRA
18S_fwd	GCCCGAAGCGTTTACTTTGA
18S_rev	TCCATTATTCCTAGCTGCGGTATC
18S_probe	FAM-AAAGCAGGCCCGAGCCGCC-TAMRA
<b>Oligos for T7 synthesis of crRNAs</b>	
T7_fwd	GAAATTAATACGACTCACTATAGG
BKV_STA_rev	CTGTGTGAAGCAGTCAATGCAGTAGCAAGTTTTAGTCCCTTCGTTTTTGGGGTAGTCTAAATCCCTATAGTGAGTCGTATTAATTC
CMV_UL54_rev	CGCGTCAGCGGATCCACACGGACCTCGTGTTTTAGTCCCTTCGTTTTTGGGGTAGTCTAAATCCCTATAGTGAGTCGTATTAATTC
CXCL9_rev	GCCCTTCCTGCGAGAAAATTGAAATCATGTTTTAGTCCCTTCGTTTTTGGGGTAGTCTAAATCCCTATAGTGAGTCGTATTAATTC
<b>Synthetic targets</b>	
CXCL9	GAAATTAATACGACTCACTATAGGATGAAGAAAAGTGGTGTCTTTTCCTCTTGGGCATCATCTTGGCTGGTTCTGATGGAGTGCAAGGAACCCAGTAGTGAGAAAGGGTCGCTGTTCTGCATCAGCACCAACCAAGGACTATCCACCTACAATCCTTGAAAGACCTTAAACAATTTGCCCAAGCCCTTCCTGCGAGAAAATTGAAATCATTGCTACACTGAAGAATGGAGTTCAAACATGTCTAAACCCAGATTTCAGCAGATGTGAAGGAAGTATTAAGGAGTGGGAGAAACAGGTCAGCCAAAAGAAAAGCAAAGAATGGGAAAAAACATCAAAAAAGAAAGTTCTGAAAGTTCGAAAATCTCAACGTTCTCGTCAAAGAAGACTACATAA
<b>Cleavage Reporter</b>	
Lateral Flow	6FAM-mArArUrGrGrCmAmArArUrGrGrCmA-BIO
Fluorescence	RNAse ALERT V2 (Thermo)

Red indicates the T7 promoter sequence